Quantum Information and Computation, Vol. 5, No. 4&5 (2005) 318–334

COHERENT OPTICAL CONTROL OF ELECTRONIC EXCITATIONS IN FUNCTIONALIZED SEMICONDUCTOR NANOSTRUCTURES

L. G. C. REGO
Department of Physics, Universidade Federal de Santa Catarina, Florianopolis, SC, 88040-900, Brazil

S. G. ABUABARA, V. S. BATISTA[a]
Department of Chemistry, Yale University, P.O.Box 208107 New Haven, CT, 06520-8107, USA

Received December 7, 2004
Revised April 26, 2005

The feasibility of creating and manipulating coherent quantum states on surfaces of functionalized semiconductor nanostructures is computationally investigated. Quantum dynamics simulations of electron-hole transfer between catechol molecules adsorbed on TiO_2 -anatase nanostructures under cryogenic and vacuum conditions indicate that laser induced coherent excitations can be prepared and manipulated to exhibit controllable spatial Rabi oscillations. The presented computational methods and results are particularly relevant to explore the basic model components of quantum-information electro-optic devices based on inexpensive and readily available semiconductor materials.

Keywords: coherent control, wave-packet dynamics, adsorbates, semiconductors
Communicated by: P Brumer

1 Introduction

The optical and mechanical manipulation of individual molecules has become a routine practice in many laboratories, holding great promise for several areas of science and technology [1, 2, 3, 4, 5]. Molecules exhibit an enormous diversity of structures and electronic properties. Once combined with solid state systems, they fit at the nanometer scale yielding their intrinsic properties to the functionalized host substrate material. Single molecules have already become the active part of nanoelectronic circuits [3] and have also been used for quantum-information processing [4]. In addition to nuclear spin states [4, 6], molecular vibrational modes have also been proposed for quantum bit (qubit) implementations [5]. However, the scalability of quantum information processing systems based on individual molecules in gases or liquids is expected to be hindered by molecular diffusion, leading to leakage and decoherence. In order to overcome these limitations, several solid-state qubit implementations are currently being pursued, including designs based on polarization states of electrons confined to quantum dots [7] and nuclear spin states of atomic impurities in semiconductor matrices [6]. Furthermore, quantum logic gates based on coupled quantum dots, treated as artificial molecules, have already been explored [8].

[a] Alfred P. Sloan Fellow

In this work we investigate the feasibility of creating and coherently manipulating quantum states in functionalized semiconductor nanostructures, in an effort to explore realistic models of molecular qubits based on *existing* semiconductor materials. *Ab-initio* molecular dynamics simulations are combined with semi-empirical electronic structure calculations in order to investigate electron-hole states, created by photoexcitation of catechol molecules functionalizing TiO_2-anatase nanostructures (see Fig. 1). TiO_2-anatase, functionalized with catechol molecules, constitutes an inexpensive material that has already been characterized both theoretically [9, 13, 14] and experimentally [10, 11, 12], serving as a simple prototype model system upon which more complex molecular structures can be attached for specific photo-transduction applications [15].

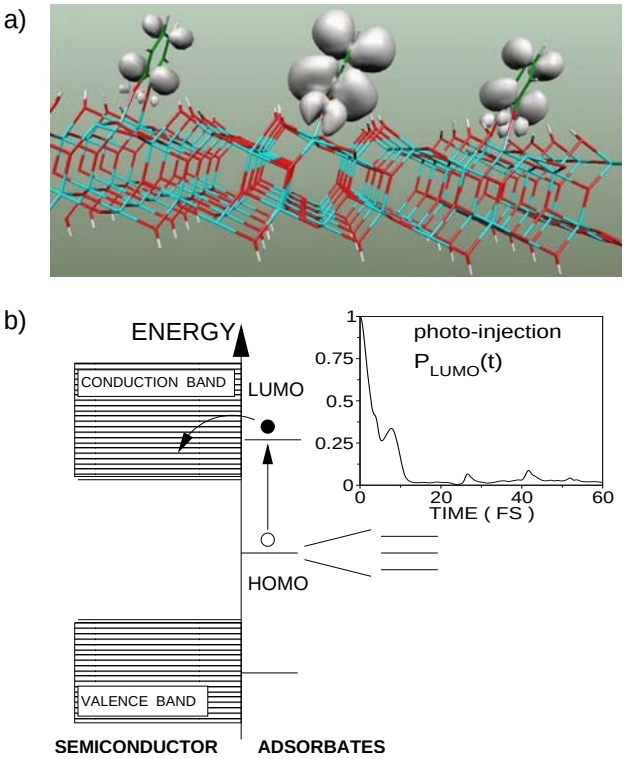

Fig. 1. a) TiO_2-anatase functionalized with catechol molecules and density isosurface representing a nonstationary hole state delocalized on the molecular adsorbates. b) Energy diagram and photo-injection process depicted by arrows, including the splitting of closely lying HOMO energy levels. The inset shows the evolution of the time-dependent electronic population during electron injection from a photo-excited catechol adsorbate [13, 14].

Functionalization results from the adsorption of molecules onto the semiconductor surface. As a result, surface complexes are formed and electronic states are introduced in the semiconductor band gap, sensitizing the host material for photo-absorption at frequencies characteristic of the molecular adsorbates (see energy level diagram in Fig. 1b). Photoexcitation of surface complexes often leads to femtosecond interfacial electron injection (see inset in Fig. 1b and arrows in the energy diagram) when there is suitable energy match between the photoex-

cited molecular state and the electronic states of the conduction band in the semiconductor material [13, 14, 16, 17, 18]. Such a photoexcitation and relaxation process has already raised significant interest for a broad range of technological developments [19]. Here, we investigate an unexplored aspect of this fundamental process involving the dynamics of hole states left within the semiconductor band gap after photoinduced electron injection [14]. The distinctive characteristic of the interband states hosting electron-holes is that they remain off-resonance relative to the semiconductor valence and conduction bands. It is therefore of interest to explore the nontrivial question as to whether such an off-resonance condition can preserve quantum coherences, despite the partial intrinsic decoherence induced by thermal ionic motion, allowing for coherent optical manipulation of hole states with available femtosecond-pulse technology. This paper investigates such a problem in terms of quantum dynamics computations based on an approximate mixed quantum-classical approach (*i.e.*, Ehrenfest mean-field nuclear dynamics) where the electrons are treated quantum mechanically and the nuclei evolve classically. The appreciation of conditions under which quantum coherences may be described according to mixed quantum-classical methodologies has been the subject of intense research [20, 21, 22, 23], including the analysis of decoherence in similar composite models [24, 25]. The applicability of mixed quantum-classical dynamics is found to be valid so long as the quantum subsystem (electronic dynamics) decoheres slowly and the remainder (nuclear dynamics), often coupled to a thermal bath, decoheres quickly [26].

2 Methods

2.1 Electronic Structure Methods

We consider simulations of quantum dynamics in a model system composed of catechol molecules adsorbed on the [101] surface of TiO_2-anatase nanostructures under cryogenic and vacuum conditions (see Figure 1a). The dimensions of the functionalized nanoparticle are 3.1 nm $\times$ 1.5 nm $\times$ 3.1 nm, along the [-101], [010] and [101] directions, respectively, with adjacent adsorbates 1.0 nm apart from each other. For future reference, the three molecular adsorbates Ω are denoted Left (L), Central (C) and Right (R) adsorbates. The optimized geometry is obtained, according with our previous studies, by geometry optimization with respect to the coordinates of the anchored catechol molecules and the TiO_2 surface [13, 14]. Geometry relaxation is performed by using the Vienna *Ab-initio* Simulation Package (VASP/VAMP) [27, 28], which implements the density functional theory (DFT) in a plane wave basis set, with the Perdew-Wang [29] generalized gradient approximation (GGA) and ultrasoft Vanderbilt pseudopotentials [30]. An ensemble of thermal configurations and nuclear trajectories is obtained by performing *ab initio* molecular dynamics simulations.

The electronic structure of the 3 nm particles is described according to a tight-binding model Hamiltonian gained from the extended Hückel (EH) approach [31, 32]. Advantages of this method are that it requires a relatively small number of transferable parameters and is capable of providing accurate results for the energy bands of elemental materials (including transition metals) as well as compound bulk materials in various phases [32]. In addition, the EH method is applicable to large extended systems and provides valuable insight on the role of chemical bonding [33]. The EH method is therefore most suitable to develop a clear chemical picture of the underlying relaxation dynamics at the semiquantitative level, including

fundamental insight on the role that symmetry plays in the localization of holes on catechol molecular orbitals (MOs)(*i.e.*, states with negligible overlap with d orbitals of nearby Ti^{4+} ions in the TiO_2 host substrate).

The EH Hamiltonian is computed in the basis of Slater-type orbitals χ for the radial part of atomic orbital (AO) wavefunctions [13, 14], including the 4s, 4p and 3d atomic orbitals of Ti^{4+} ions, the 2s and 2p atomic orbitals of O^{2-} ions, the 2s and 2p atomic orbitals of C atoms, and the 1s atomic orbitals of H atoms. The AOs $\{|\chi_i(t)\rangle\}$ form a mobile (nonorthogonal) basis set due to nuclear motion, with $S_{ij}(t) = \langle\chi_i(t)|\chi_j(t)\rangle$ the corresponding time-dependent overlap matrix elements. The overlap matrix is computed using periodic boundary conditions along the [010] direction.

Diagonalization of the EH Hamiltonian predicts a 3.3 eV band gap for the 3.0 nm model system in its relaxed configuration. This result is consistent with the experimental value of 3.2 eV for the band gap of bulk TiO_2-anatase, 3.4 eV for 2.4 nm particles [34], and 3.7 eV band gap for the 1.2 nm model system [13], since the smaller the nanoparticle the larger is the band gap.

2.2 Quantum Dynamics Methods

We confine ourselves to an approximate mixed quantum-classical method in which the electrons are treated quantum mechanically and the nuclei classically. The nuclei evolve on an effective mean-field Born-Oppenheimer potential energy surface (PES), V_{eff}, according to classical trajectories $\mathbf{R}^\xi = \mathbf{R}^\xi(t)$ with initial conditions specified by the index ξ. The time-dependent electronic wave function is propagated for each nuclear trajectory $\mathbf{R}^\xi(t)$, according to a numerically exact integration of the Time-Dependent Schrödinger Equation (TDSE),

$$\{\frac{\partial}{\partial t} + \frac{i}{\hbar}\hat{\mathbf{H}}(t)\}|\Psi^\xi(t)\rangle = 0. \tag{1}$$

Here, $\mathbf{H}(t)$ is the electronic EH Hamiltonian which depends on t through $\mathbf{R}^\xi(t)$. The actual calculation of V_{eff}, or equivalently of the set of trajectories $\mathbf{R}^\xi(t)$, is a difficult problem [35]. However, in the present application both the ground and excited electronic state PESs involve bound nuclear motion of similar frequencies. Therefore, V_{eff} is nearly parallel to the ground state PES. Nuclear trajectories $\mathbf{R}^\xi(t)$ are therefore approximated according to *ab initio*-DFT Molecular Dynamics simulations.

Results reported in Sec. 3 are obtained, according to the resulting propagation scheme, by sampling initial conditions ξ for nuclear motion, integrating the TDSE over the corresponding nuclear trajectories and averaging expectation values over the resulting time-evolved wavefunctions. Converged results are typically obtained with less than 50 initial conditions representing the system thermalized under conditions of 100 K and constant volume. However, results are reported for averages of 100 initial conditions.

The TDSE, introduced by Eq. (1), is numerically integrated by expanding the time-dependent hole wavefunction

$$|\Psi^\xi(t)\rangle = \sum_q B_q(t)|\phi_q(t)\rangle, \tag{2}$$

in the basis of the instantaneous MOs

$$|\phi_q(t)\rangle = \sum_i C_{i,q}(t)|\chi_i(t)\rangle, \tag{3}$$

— *i.e.*, the instantaneous eigenstates of the generalized eigenvalue problem

$$\mathbf{H}(t)\mathbf{C}(t) = \mathbf{S}(t)\mathbf{C}(t)\mathbf{E}(t), \tag{4}$$

with eigenvalues $E_q(t)$.

The propagation scheme is based on the recursive application of the following short-time approximation:

$$|\Psi^{\xi}(t+\tau/2)\rangle \approx \sum_q B_q(t) e^{-\frac{i}{\hbar}E_q(t)\tau/2} |\phi_q(t)\rangle, \tag{5}$$

where the evolution of the expansion coefficients

$$B_q(t+\tau) = \sum_p B_p(t) e^{-\frac{i}{\hbar}[E_p(t)+E_q(t+\tau)]\tau/2} \langle \phi_q(t+\tau)|\phi_p(t)\rangle$$

is approximated as follows,

$$B_q(t+\tau) \approx B_q(t) e^{-\frac{i}{\hbar}[E_q(t)+E_q(t+\tau)]\tau/2}, \tag{6}$$

in the limit of sufficiently thin time-slices τ.

The initial hole state, after electron-hole pair separation, is the Highest Occupied Molecular Orbital (HOMO) of the photoexcited surface-complex C. The subsequent relaxation dynamics is quantitatively described in terms of the time-dependent hole populations $\mathbf{P}_{\Omega}(t)$ of the molecular adsorbates $\Omega = (L, C, R)$.

The time-dependent hole population $\mathbf{P}_{\Omega}(t)$ is computed as follows,

$$\mathbf{P}_{\Omega}(t) = \mathsf{Tr}\{\hat{\rho}(t)\hat{P}_{\Omega}\}, \tag{7}$$

where $\hat{P}_{\Omega}$ is the projection operator onto atomic orbitals of adsorbate Ω,

$$\hat{P}_{\Omega} = \sum_{k,j\in\Omega} |\chi_j\rangle S^{-1}_{jk} \langle\chi_k|, \tag{8}$$

and $\hat{\rho}(t)$ is the reduced density operator associated with the electronic degrees of freedom,

$$\hat{\rho}(t) = \sum_{\xi} p_{\xi} |\Psi^{\xi}(t)\rangle\langle\Psi^{\xi}(t)|, \tag{9}$$

where p_{ξ} is the probability of sampling the nuclear initial condition specified by index ξ.

3 Results

3.1 Rabi Oscillations

Figure 2 (left panel) shows the time-dependent populations $P_{\Omega}(t)$ of each adsorbate as a function of time (thick lines). Thin lines show the contributions of a single representative trajectory $\mathbf{R}^{\xi}$ to the total ensemble averages $\mathbf{P}_{\Omega}(t)$. Note that almost 90 % of the hole population remains localized, throughout the entire relaxation time, on those atomic orbitals belonging to the adsorbate molecules. The remaining 10 % of the hole population remains next to the molecular adsorbates, localized in the d orbitals of Ti^{4+} ions that have partial overlap with the molecular adsorbates [14]. These results are consistent with the fact that,

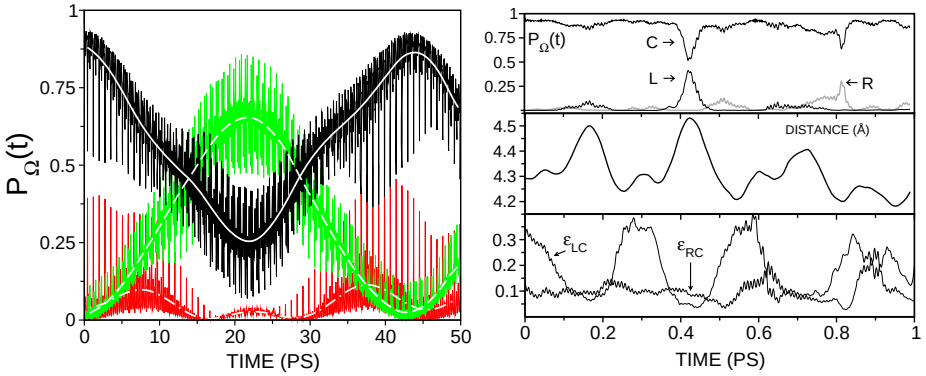

Fig. 2. Left panel: Time-dependent hole populations $\mathbf{P}_\Omega(t)$ of adsorbate molecules $\Omega = (C, R, L)$ in thick white solid, dashed, and dot-dash lines, respectively. Superimposed thin solid lines show the contribution of a single representative trajectory to the total ensemble average populations. Right top panel: Time-dependent hole population $\mathbf{P}_\Omega(t)$ of adsorbate molecules: $\Omega = C$ and $\Omega = L$ (top and bottom black lines, respectively), and $\Omega = R$ (gray line) for the early time dynamics. Right middle panel: adsorbate-semiconductor distance measured from the center-of-mass of catechol to the semiconductor surface. Right lower panel: energy difference (in meV) between near-resonant MOs.

under vacuum conditions, the recombination of injected electrons back to the molecule (back-transfer) occurs in the nanosecond time-scale [36].

Figure 2 (left panel) indicates that the hole is transferred between adjacent catechol molecules, remaining localized in the mono-layer of adsorbate molecules rather than undergoing injection into the semiconductor host substrate. The underlying hole relaxation dynamics is therefore significantly different from the relaxation of the photoexcited electron which, according to the results reported in Ref. [13] as well as in the inset of Fig. 1, is usually completely injected into the semiconductor material within a few femtoseconds.

Note that hole transfer involves adsorbates with negligible overall of AOs, since catechol molecules are anchored to the surface more than 1 nm apart from each other. However, near-resonant electronic states, localized in adjacent adsorbate molecules, are indirectly coupled by the common host-substrate giving rise the observed relaxation. Considering that there is no significant hole population transfer to the semiconductor surface, these results are consistent with a super-exchange hole transfer mechanism mediated by the semiconductor host substrate.

An approximate description of hole-tunneling between adsorbate molecules Ω and Ω', coupled by the host substrate, can be given in terms of the Rabi formulae:

$$\mathbf{P}_\Omega(t) = \frac{\gamma^2_{\Omega\Omega'}/\hbar^2}{\Gamma^2_{\Omega\Omega'}} \sin^2\left(\ \Gamma_{\Omega\Omega'}\ t\ \right), \tag{10}$$

and $\mathbf{P}_{\Omega'}(t) = 1 - \mathbf{P}_\Omega(t)$. The calculated hole-tunneling period, obtained from Fig. 2, is T $\approx$ 42 ps and has an exponential dependence with the separation between molecular adsorbates. The parameter $\Gamma_{\Omega\Omega'} = \left[(\gamma_{\Omega\Omega'}/\hbar)^2 + (\omega_{\Omega\Omega'}/2)^2\right]^{1/2}$, introduced by Eq. (10), is the Rabi frequency, $\gamma_{\Omega\Omega'}$ is the effective quantum coupling between resonant states and $\omega_{\Omega\Omega'}$ is the corresponding Bohr frequency. The parameters computed from Fig. 2 are $\omega_{LC} \approx 4.5\ \omega_{RC}$ and $\gamma_{RC} \approx 1.12\ \gamma_{LC}$. It is important to mention that the asymmetric nature of the underlying relaxation dynamics (as evidenced by the asymmetric population of the R and L

adsorbates) is primarily due to the intrinsic asymmetry of the local substrate environment that interact with each adsorbate. Such small differences determine asymmetric couplings between molecular adsorbates and a preferential direction for the hole motion.

Figure 2 (right panel) shows a detailed analysis of the early time relaxation dynamics for a representative nuclear trajectory, including the quantitative description of the adsorbate time-dependent hole populations, the evolution of the adsorbate-semiconductor distance, and the evolution of energy differences between near-resonant electronic states of surface complexes localized in the semiconductor band-gap. The analysis of these results indicates that the time-dependent populations $\mathbf{P}_\Omega(t)$ (top right panel) are correlated with the motion of the molecular adsorbates (middle right panel), since the adsorbate-semiconductor separation modulates the time-dependent energy differences ε_{RC} and ε_{LC} between the initially populated state C and the near-resonant electronic states in the R and L adsorbates, respectively (bottom right panel). The most significant population exchange, during this first picosecond of dynamics, is observed when the adsorbate-semiconductor separation reaches a maximum value, at approximately $t = 0.41$ ps (see Fig. 2, middle right panel). At that point, states L and C remain near-resonant for about 100 fs (see Fig. 2, top right panel) and exchange population without significantly populating any other state (*e.g.*, states responsible for coupling states L and C).

The extent to which these results are significant is associated with the survival of electronic coherences, responsible for the Rabi oscillations shown in Fig. 2. To this end, we examine the diagonal and off-diagonal elements of the reduced density matrix $\rho(t)$, introduced by Eq. (9), in the basis of catechol MOs. The analysis, presented in Fig. 3, is focused on the calculation of matrix elements of $\rho(t)$ associated with the HOMOs of the isolated catechol molecules L,C, and R, which can be represented in occupancy notation as register states $|100\rangle$, $|010\rangle$, and $|001\rangle$, respectively. Note that in this notation, $\hat{\rho}(0) = |010\rangle\langle 010|$. The

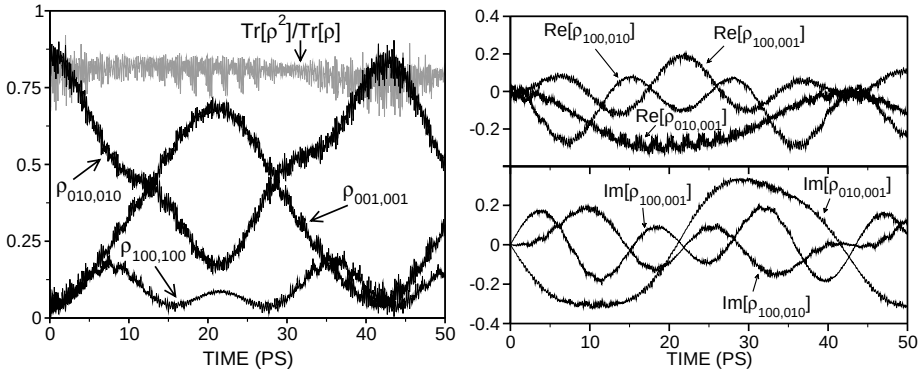

Fig. 3. Left panel: Comparison of the trace of the square of the reduced density matrix (gray curve) and the time evolution of the hole population on the surface complexes L,C,R (black curves). Ensemble averages were converged by sampling over 100 different initial conditions ξ. Right panel: Real (upper panel) and imaginary (lower panel) parts of non-zero off-diagonal matrix elements of reduced density matrix for register states $|100\rangle$, $|010\rangle$ and $|001\rangle$ demonstrating coherent super-exchange hole tunneling dynamics for the first 50 ps of dynamics.

black curves in Fig. 3 (left panel) show that the diagonal elements of the reduced density matrix for states $|100\rangle$, $|010\rangle$ and $|001\rangle$ correspond closely to the total adsorbate populations

$\mathbf{P}_L(t)$, $\mathbf{P}_C(t)$ and $\mathbf{P}_R(t)$ reported in Fig. 2, indicating that most of the hole population remains localized in these adsorbate states throughout the simulation time. Furthermore, the non-zero off-diagonal elements, shown in Fig. 3 (right panel), demonstrate that the hole relaxation dynamics remains remarkably coherent for the entire simulation time despite thermal nuclear motion. (Note: For clarity, results are presented for the first 50 ps of dynamics. It is, however, important to mention that our calculations indicate that both Rabi oscillations and quantum coherences are preserved for at least hundreds of picoseconds.)

The observed coherent localization in the space of electronic states is mainly due to the finite size of the nanostructure, where the register states are coupled by the common host substrate but remain off-resonant relative to valence and conduction bands (manifolds) of electronic states [13]. In contrast, the analogous relaxation dynamics on extended systems is expected to delocalize the hole excitation on the manifold of near-resonant electronic states introduced by the adsorbate molecules. Hole excitations in disordered extended systems with low surface coverage, however, are expected to have an intermediate behavior and exhibit localized coherent relaxation within small disjoint islands of adsorbate molecules.

A quantitative measure of intrinsic decoherence (see Fig. 3, left panel) is obtained by computing the trace of the square of the reduced density matrix $\mathsf{Tr}[\rho^2(t)]$ [37, 38, 39]. We refer to the decoherence induced by the nuclear motion on the quantum subsystem as *intrinsic decoherence* to make a distinction from cases where decoherence is caused by the direct coupling of the quantum subsystem with an external bath. Such a quantity measures the decay of purity as the initial state becomes a statistical mixture of electronic states due to decoherence induced by thermal nuclear motion. The gray curve in Fig. 3 (left panel) shows that $\mathsf{Tr}[\rho^2(t)]$ decays about 15 % at very early times due to partial mixing in the initially photoexcited surface complex C. However, throughout the rest of the propagation time, $\mathsf{Tr}[\rho^2(t)]$ remains approximately constant, decaying at a much lower rate while the hole tunnels between adjacent molecular adsorbates. These results thus indicate that the underlying hole relaxation dynamics remains highly coherent on the surface of the nanoparticle in spite of thermal nuclear motion.

3.2 Model System

The analysis of spatial Rabi oscillations, presented in Sec. 3.1, indicates that coherent superexchange hole transfer between adsorbate molecules attached to TiO_2 semiconductor nanostructures results from multiple scattering events where near-resonant states localized in adsorbate molecules become indirectly coupled by intermediate states in the semiconductor host substrate. Coupling events last for about 100 fs and occur once or twice every ps as thermal fluctuations modulate the electronic couplings and the resonance conditions (see Fig. 2, right panel). It is, therefore, natural to expect that similar coherent Rabi oscillations should be observable in other systems, whenever donor and acceptor states become indirectly coupled by mediating states, so long as the life-time of the mediating state is longer than the duration of a single scattering event.

In order to explore this fundamental aspect of the observed quantum coherent Rabi oscillations, consider the simplest possible implementation of multiple STImulated Raman Adiabatic Passage (STIRAP) events [40, 41, 42, 43, 44] in the three-level system depicted in Fig. 4,

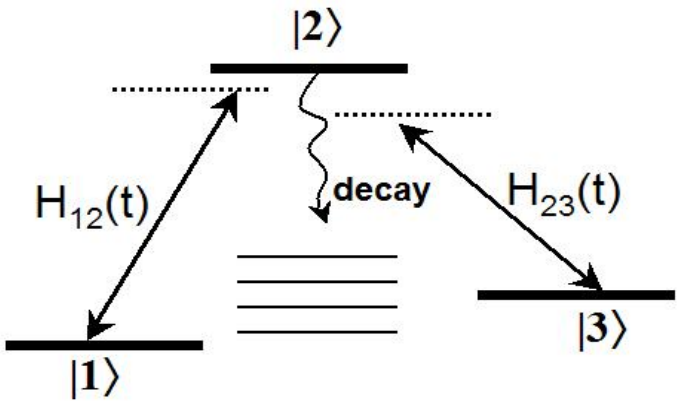

Fig. 4. Three-level excitation model scheme [40]. States $|1\rangle$ and $|3\rangle$ are coupled by a train of Stokes and pump laser pulses, described by $H_{23}(t)$ and $H_{12}(t)$, respectively, slightly detuned relative to the intermediate state $|2\rangle$. The life-time of state $|2\rangle$ is longer than the duration of the pulses.

described by the following time-dependent model Hamiltonian,

$$H(t) = \begin{pmatrix} E_1 & H_{12}(t) & 0 \\ H_{12}(t) & E_2 & H_{23}(t) \\ 0 & H_{23}(t) & E_3 \end{pmatrix}, \tag{11}$$

written in the basis of states $|1\rangle$, $|2\rangle$ and $|3\rangle$, with $E_1 = 0$ meV, $E_2 = 28.60$ meV and $E_3 = 5.72$ meV, respectively. The coupling strength between states is determined by a train of femtosecond pump and Stokes pulses described by $H_{12}(t)$ and $H_{23}(t)$ (*vide infra*). These pulses induce population exchange between states $|1\rangle$ and $|3\rangle$, according to standard three-state two-photon Raman processes, leaving $|2\rangle$ without any significant population. When using the Schrödinger equation to describe time evolution, spontaneous decay from $|2\rangle$ is accounted for by adding an imaginary component to the excited-state energy E_2, corresponding to the decay rate into states other than $|1\rangle$ and $|3\rangle$.

Note that here, in analogy to the adsorbate states in the semiconductor nanostructure, donor and acceptor states ($|1\rangle$ and $|3\rangle$) are only indirectly coupled by the mediating state $|2\rangle$, as modulated by $H_{12}(t)$ and $H_{23}(t)$. Starting with population in state $|1\rangle$, the counterintuitive order of pulses is implemented with the Stokes pulse $H_{23}(t)$ preceding the pump pulse $H_{12}(t)$ as indicated in Fig. 5 (right lower panel), first coupling the acceptor $|3\rangle$ and intermediate state $|2\rangle$, and then coupling the donor $|1\rangle$ and intermediate $|2\rangle$. Here, $H_{23}(t)$ and $H_{12}(t)$ are Gaussian pulses, depicted in Fig. 5 (right lower panel), with a pulse-width of 134 fs and a relative pulse delay of 138 fs. Such a coupling scheme transfers population between $|1\rangle$ and $|3\rangle$ without significantly populating state $|2\rangle$ (see Fig. 5, right upper panel). While the pulse delay and coupling strengths could be adjusted in order to achieve partial or complete population transfer between $|1\rangle$ and $|3\rangle$ without losing population by spontaneous emission from state $|2\rangle$, parameters have been chosen in order to mimic the time-dependent populations

shown in Fig. 2. Under typical experimental conditions, there might be some diabatic loss of population to $|2\rangle$, but this should not significantly affect the overall transfer mechanism. Figure 5 (left panel) shows the evolution of time-dependent populations $\mathbf{P}_\Omega(t)$ that result from extending such a coupling scheme periodically with a period of about 1.72 ps. Analogously to the relaxation dynamics observed in functionalized semiconductor nanostructures (see Fig. 2, left panel), coherent Rabi oscillations are observed with periodicity of about 42 ps.

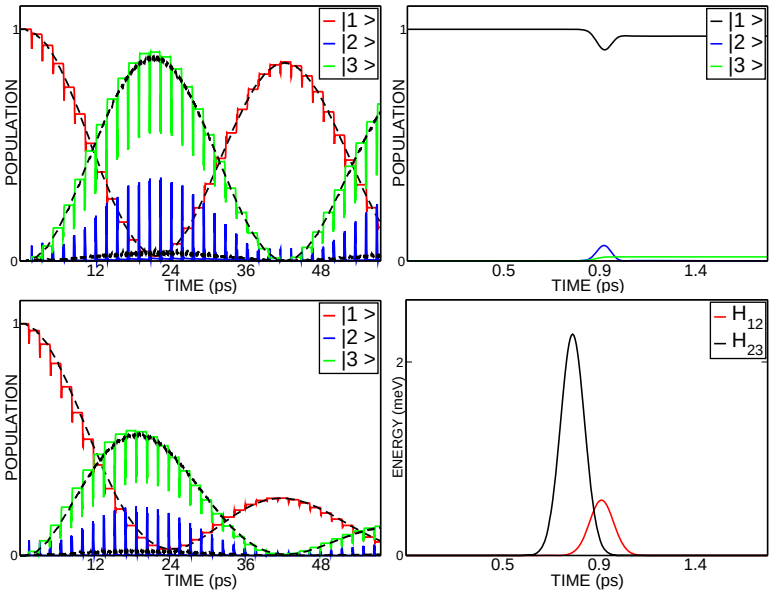

Fig. 5. Left panels: Time-dependent populations $\mathbf{P}_\Omega(t)$ of states $\Omega = |1\rangle$, $|2\rangle$ and $|3\rangle$ for the 3-level STIRAP system depicted in Fig. 4. Thin lines show the contribution of a single representative trajectory to the total ensemble average of 200 realizations of dynamics indicated by black dashed lines. The finite life-time of intermediate state $|2\rangle$ is $\tau_2 = 10$ ps (left top panel) and $\tau_2 = 1$ ps (left lower panel). Time-dependent populations show repeated partial transfer due to the train of pump and Stokes laser pulses, described by $H_{12}(t)$ and $H_{23}(t)$, inducing multiple STIRAP events throughout the whole relaxation time. Right top panel: Time-dependent populations $\mathbf{P}_\Omega(t)$ during the early time dynamics. Right lower panel: counterintuitive order of coupling pump and Stokes pulses, $H_{12}(t)$ (red) and $H_{23}(t)$ (black), respectively.

The comparison between Fig. 5 and Fig. 2 provides insight into the underlying hole-relaxation mechanism observed in semiconductor nanostructures. It is concluded that thermal fluctuations transiently couple the otherwise energetically isolated states of adjacent adsorbates to MOs delocalized in the nanostructure, mediating population transfer between spatially isolated adsorbate states according to multiple STIRAP-like events. The robustness of the observed Rabi oscillation is found to rely upon the life-time of the mediating state, which must be longer that the duration of a single coupling event.

The similarity between the relaxation dynamics induced by multiple STIRAP events in the three-level model system and the quantum coherent Rabi oscillations induced by thermal nuclear motion in the functionalized TiO_2 semiconductor nanostructure allows for the analysis of the influence of dephasing on the underlying transfer mechanism. The feasibility

of STIRAP events under the influence of pure dephasing has been investigated by several authors, reporting conditions for which the efficiency of adiabatic passage approaches its dephasing-free value [42, 43, 44]. These findings suggest that STIRAP-like processes should be feasible not only in vacuum but also in condensed-phase environments (*e.g.*, solutions). In general, however, the prospect of adiabatic passage depends on the details of the dephasing mechanism. In particular, correlated dephasing in state $|2\rangle$ immediately following a coupling event does not significantly affect the population transfer since state $|2\rangle$ has negligible population at times between coupling events. There is, however, the nontrivial question as to

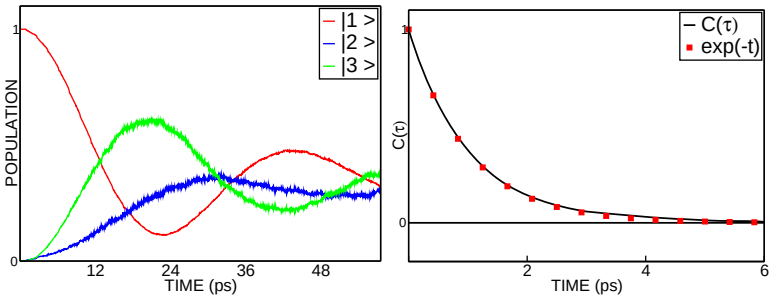

Fig. 6. Left panel: Time-dependent populations $\mathbf{P}_\Omega(t)$ of states $\Omega = |1\rangle$, $|2\rangle$ and $|3\rangle$ for an average of 200 realizations of dynamics in the 3-level STIRAP system depicted in Fig. 4 in the presence of spontaneous uncorrelated dephasing with a 1 ps timescale, implemented as described in the text. Right panel: Autocorrelation function of the phase of state $|2\rangle$ due to spontaneous uncorrelated dephasing with a 1 ps timescale.

whether the observed Rabi oscillations would be preserved under *uncorrelated* dephasing in state $|2\rangle$. Analogously to simulations of spontaneous population decay from state $|2\rangle$, the effect of spontaneous uncorrelated dephasing is computationally investigated in the three-level model system by adding a random phase to state $|2\rangle$ at a random time (on average once a ps), when using the Schrödinger equation to describe time evolution. Figure 6 shows that even under these detrimental conditions of uncorrelated dephasing within a ps timescale the system still exhibits Rabi oscillations due to population transfer between states $|\ 1\rangle$ and $|\ 3\rangle$ with a period of about 42 ps. In contrast to super-exchange transfer, however, such a dephasing mechanism populates the mediating state $|2\rangle$. These results indicate that the observed Rabi oscillations should be observable even in the presence of uncorrelated dephasing with a 1 ps timescale.

3.3 Optical Coherent Control

This section investigates the feasibility of achieving coherent control of the underlying superexchange hole transfer relaxation responsible for the coherent Rabi oscillations discussed in Secs. 3.1 and 3.2. The specific coherent-control scheme implemented involves a sequence of ultrashort laser pulses that couple a populated state in an adsorbate molecule with an auxiliary state, inducing a sequence of π phase-shifts in the time-evolved wave-packet component corresponding to the initially populated state of interest. Such a coherent control scenario is inspired in other successful approaches for modulating quantum relaxation dynamics based on multiple pulses [45, 46, 47, 48, 49]. All of these approaches are particularly suited for ap-

plications to quantum information processing since they preserve the coherent nature of the unitary evolution. In contrast, other approaches proposed to control decay of excited states are based on the frequent *collapse* (*i.e.*, measurement) of the time-dependent wavefunction [50, 51] and therefore do not preserve the coherent nature of quantum dynamics.

In the present implementation, the time evolution operator that describes the transformation due to a single ultrashort 2π-pulse is

$$\hat{U}_{2\pi} = \hat{\mathbf{I}} - 2\frac{\mid 010\rangle\langle 010 \mid}{\langle 010 \mid 010\rangle} \ , \tag{12}$$

where $\hat{\mathbf{I}}$ is the identity operator and $\mid 010\rangle$ is the initially populated state. Therefore, the transformed wavefunction after applying a 2π-pulse to the time-evolved wavefunction $|\Psi_t\rangle$ is $\mid \Psi_t^{(2\pi)}\rangle = \hat{U}_{2\pi} \mid \Psi_t\rangle$. We proceed to investigate the effect of a sequence of ultrashort 2π pulses on the relaxation of the time-dependent wave-packet, considering that the width of the 2π pulses is much shorter than the interval τ between pulses ($\tau = 550\ fs$).

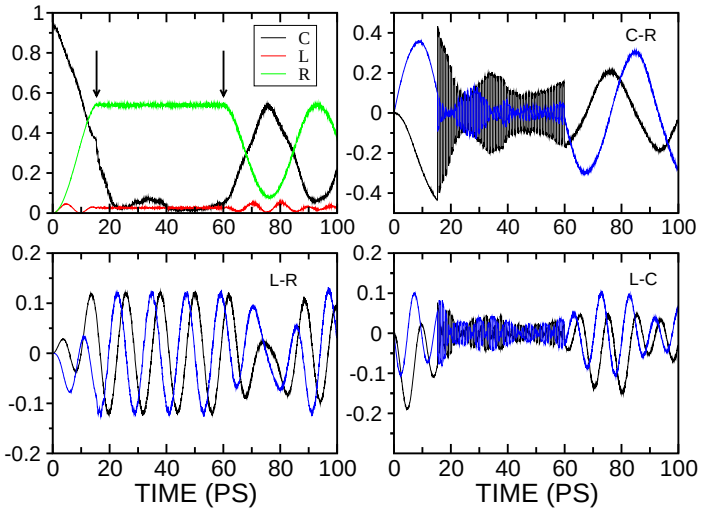

Fig. 7. Upper-left panel: hole population P_Ω for the three adsorbates; arrows indicate the start and the end of the sequence of pulses. Other panels show the real (black) and imaginary (blue) parts of the off-diagonal density matrix elements, indicated by labels.

Figure 7 illustrates the perturbational effect of a sequence of ultrashort 2-π pulses on the hole relaxation dynamics during the first 100 ps of dynamics. The 2-π pulses are applied in the $t = 15$—60 ps time window (indicated with arrows) at intervals of 550 fs, starting at $t_i = 15\ ps$ when there is maximum entanglement between adsorbates C and R (*i.e.*, when $|\rho_{010,001}|$ is maximum). Figure 7 shows the resulting time-dependent hole populations $P_\Omega(t)$ (upper-left panel). The other panels show the matrix elements of the time-dependent reduced density matrix $\rho^{3\times 3}_{\Omega,\Omega'}(t)$, in terms of real (black) and imaginary (blue) components associated with the pairs of states indicated by the labels. These are the most significant matrix elements since,

according to Sec. 3.1, the subset of adsorbate states $(L, C, R = |100\rangle, |100\rangle, |100\rangle)$ localize most of the hole population throughout the relaxation dynamics.

The main effect of the optical pulses is to suspend Rabi oscillations, keeping constant the population of adsorbate R. Population locking results from the highly oscillatory evolution of the off-diagonal matrix elements $\rho_{010,001}$ and $\rho_{100,010}$, due to the perturbational effect of the pulses, affecting the interference with mediating intermediate states. However, since coherences are intrinsically preserved, the system is able to re-establish the coherent Rabi oscillations once the sequence of pulses is over at 60 ps.

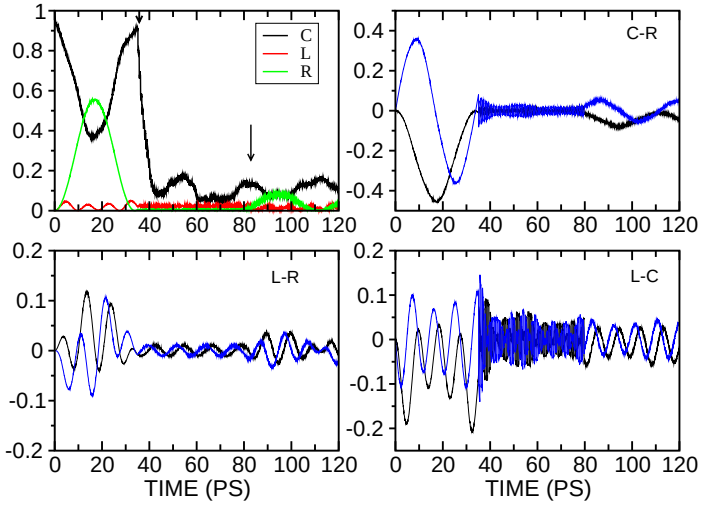

Fig. 8. Upper-left panel: hole population P_Ω for the three adsorbates; arrows indicate the start and the end of the sequence of pulses. Other panels show the real (black) and imaginary (blue) parts of the off-diagonal density matrix elements, indicated by labels.

It is important to note that the resulting dynamics, generated by a sequence of 2π pulses, strongly depends on the position along the Rabi cycle where the sequence of pulses starts acting on the system (*i.e.*, the time when the train of 2-π pulse is 'turned on'). In order to illustrate this aspect, we consider starting the sequence of pulses at a time when there is minimum entanglement between adsorbates C and R adsorbates (*i.e.*, when $|\rho_{010,001}|$ is small). Figure 8 shows that the resulting time-dependent hole populations $P_\Omega(t)$ (upper-left panel) are significantly different from those shown in Fig. 7, resulting from a different start for sequence of pulses. Figure 8 also shows more evidently that while the sequence of pulses is acting on the system the initially populated state, $C = |010\rangle$, interferes with states in the semiconductor structure partially injecting hole population. Therefore, when the sequence of pulses is over, Rabi oscillations are re-established but with a reduced amplitude.

4 Summary and Conclusions

We have shown that mixed quantum-classical simulations, based on *ab initio*-DFT Molecular Dynamics, can be efficiently implemented to simulate quantum electronic dynamics, revealing

the feasibility of super-exchange hole tunneling dynamics in a model study of functionalized TiO_2-anatase nanostructure under cryogenic and vacuum conditions. It is found that quantum coherences, between hole states localized energetically deep in the semiconductor band gap, can persist for hundreds of picoseconds despite the partial intrinsic decoherence induced by thermal ionic motion. The observed coherent hole population transfer among adjacent adsorbates is mainly stabilized by the finite size of the nanostructure, where register states are coupled by the common host substrate but remain off-resonant relative to the valence and conduction bands (manifolds) of electronic states. Carrier-phonon, and likely carrier-carrier, scattering mechanisms which would otherwise lead to the commonly observed ultrafast decoherence in semiconductor spectroscopy [52] are highly suppressed by the off-resonance and symmetry conditions of the electronic states in surface complexes. It is concluded that the predicted observation of Rabi oscillations, associated with adsorbate electronic populations, could provide a simple experimental probe of coherent quantum relaxation dynamics associated with super-exchange hole transfer. Considering the great technological interest in encoding and manipulating quantum states in inexpensive and readily available semiconductor materials [53], we anticipate significant experimental interest in examining the predicted relaxation dynamics reported in this paper.

We have investigated the feasibility of coherently controlling the underlying hole relaxation dynamics by multiple 2-π pulses. The reported results suggest that functionalized TiO_2 semiconductor materials can be photo-excited to exhibit coherently controllable spatial Rabi oscillations, possibly offering a readily available platform to encode logical hole states within the subspace of adsorbate surface complexes. Such a subset of adsorbates states seem to offer symmetry and off-resonance conditions suitable to protect the evolution of quantum states against the decoherence effect of the lattice motion, naturally providing a passive error prevention scheme [54]. The reported calculations associated with functionalized TiO_2-anatase nanostructures (and mimic 3-level multiple STIRAP system) indicate that coherent wavepacket dynamics, resulting from multiple scattering events between states indirectly coupled by intermediate states, could be preserved for hundreds of picoseconds whenever the lifetime of the mediating intermediate state is longer than the duration of each scattering event. Finally, we conjecture that the ability to assemble molecules on a nanostructure solid surface, together with the rich variety of properties characteristic of potential molecular adsorbates, make functionalized semiconductors a promising alternative for the construction of quantum information photo-optic devices.

Acknowledgments

L.G.C. Rego acknowledges the financial assistance from CAPES/Brazil, under the PRODOC program. V.S.B. acknowledges supercomputer time from the National Energy Research Scientific Computing (NERSC) Center and financial support from Research Corporation, Research Innovation Award # RI0702, a Petroleum Research Fund Award from the American Chemical Society PRF # 37789-G6, a junior faculty award from the F. Warren Hellman Family, the National Science Foundation (NSF) Career Program Award CHE # 0345984, the NSF Nanoscale Exploratory Research (NER) Award ECS # 0404191, an Alfred P. Sloan fellowship from the Sloan foundation and start-up package funds from the Provost's office at Yale University.

References

1. C. Hettich et al (2002), *Nanometer resolution and coherent optical dipole coupling of two individual molecules*, Science **298** 385.
2. For a series of review articles on single molecule physics refer to Science **283** (March 1999).
3. C. Joachim et al. (2000), Nature **408**, 541; J. Park et al. (2002), Nature **417**, 722; W. Liang et al. (2002), Nature **417** 725.
4. L.M.K. Vandersypen (2001), *Experimental realization of Shor's quantum factoring algorithm using nuclear magnetic resonance*, Nature **414**, 883.
5. C.M. Tesch (2002), *Quantum computation with vibrationally excited molecules*, Phys. Rev. Lett. **89**, 157901.
6. B.E. Kane (1998), *A silicon-based nuclear spin quantum computer*, Nature **393** 133.
7. X.Q. Li, Y.W. Wu, D. Steel, et al. (2003), *An all-optical quantum gate in a semiconductor quantum dot*, Science **301** 809.
8. M. Bayer et al.(2001), *Coupling and entangling of quantum states in quantum dot molecules*, Science **291**, 451.
9. D.E. Wheeler et al. (1999), *Density functional theory analysis of electronic structure variations across the orthoquinone/semiquinone/catechol redox series*, J. Chem. Phys. A **103**, 4101.
10. Y. Liu et al. (1999), *Study of interfacial charge-transfer complex on TiO_2 particles in aqueous suspension by second-harmonic generation*, J. Phys. Chem. B **103**, 2480.
11. J. Moser, S. Punchihewa, P.P. Infelta, and M. Gratzel (1991), *Surface complexation of colloidal semiconductors strongly enhances interfacial electron-transfer rates*, Langmuir **7**,3012.
12. R. Rodriguez, M.A. Blesa, and E. Regazzoni (1996), *Surface complexation at the TiO_2 (anatase) aqueous solution interface: Chemisorption of catechol*, J. Colloidal Interface. Sci. **177**, 122 (1996).
13. L.G.C. Rego and V.S. Batista (2003), *Quantum dynamics simulations of interfacial electron transfer in sensitized TiO_2 semiconductors*,J. Am. Chem. Soc. **125**, 7989.
14. L.G.C. Rego, S.G. Abuabara, and V.S. Batista (2005), *Coherent quantum dynamics of hole states in functionalized semiconductor nanostructures*, J. Chem. Phys. **122**, 154709.
15. C. R. Rice et al. (2000), *Catechol as an efficient anchoring group for attachment of ruthenium-polypyridine photosensitisers to solar cells based on nanocrystalline TiO_2 films*, New J. Chem.**24**, 651.
16. J. Schnadt et al. (2002), *Experimental evidence for sub-3-fs charge transfer from an aromatic adsorbate to a semiconductor*, Nature **418**, 620.
17. R. Huber et al. (2002), *Real-time observation of photoinduced adiabatic electron transfer in strongly coupled dye/semiconductor colloidal systems with a 6 fs time constant*, J. Phys. Chem. B **106**, 6494.
18. J.B. Asbury et al. (2001), *Ultrafast electron transfer dynamics from molecular adsorbates to semiconductor nanocrystalline thin films*, J. Phys. Chem. B **105**, 4545.
19. B. O'Regan and M. Grätzel, Nature **353**, 737 (1991); *ibid.* **414** 338 (2001); A.H.M. Grätzel, Acc. Chem. Res. **33**, 269 (2000). For a review refer to R.J.D. Miller, G. McLendon, A. Nozik, F. Willing, and W. Schmickler, in *Surface Electron-Transfer Processes* (VCH, New York,1995).
20. W.H. Zurek (1981), *Pointer basis of quantum apparatus - Into what mixture does the wave packet collapse ?*, Phys. Rev. D **24**, 1516.
21. W.H. Zurek (1982), *Environment - Induced super-selection rules*, Phys. Rev. D **26**, 1862.
22. E. Joos and H.D. Zeh (1985), *The emergence of classical properties through interaction with the environment*, Z. Phys. B: Condens. Matter **59**, 223.
23. E. Joos, H.D. Zeh et al. (1996), *Decoherence and the Appearance of a Classical World in Quantum Theory*, Springer-Verlag, Berlin Heidelberg.
24. E.R. Bittner and P.J. Rossky (1995), *Quantum decoherence in mixed quantum-classical systems - nonadiabatic processes*, J. Chem. Phys. **103**, 8130.
25. O.V. Prezhdo and P.J. Rossky (1998), *Relationship between quantum decoherence times and solvation dynamics in condensed phase chemical systems*, Phys. Rev. Lett. **81**, 5294.
26. K. Shiokawa and R. Kapral (2002), *Emergence of quantum-classical dynamics in an open quantum environment*, J. Chem. Phys. **117**, 7852.

27. http://cms.mpi.univie.ac.at/vasp/.
28. G. Kresse (1996), *Efficient iterative schemes for ab initio total-energy calculations using a plane-wave basis set*, Phys. Rev. B **54**, 11169.
29. J. Perdew, in *Electronic Structure of Solids*, P. Ziesche and H. Eschrig eds. (Verlag, Berlin, 1991).
30. D. Vanderbilt (1990), *Soft self-consistent pseudopotentials in a generalized eigenvalue formalism*, Phys. Rev. B **41**, 7892.
31. S.P.Mc. Glynn and L.G. Vanquickenborne and M. Kinoshita and D.G. Carroll (1972) *Introduction to Applied Quantum Chemistry*, Holt, Ed., Rinehart and Winston INC., New York.
32. J. Cerdá and F. Soria (2000), *Accurate and transferable extended Hückel-type tight-binding parameters*, Phys. Rev. B **61**, 7965.
33. R. Hoffmann (1988), Rev. Mod. Phys. **60** 601; J.H. Ammeter et al. (1978), , J. Am. Chem. Soc. **100**, 3686.
34. C. Kormann, D.W. Bahnemann and M.R. Hoffmann (1988), *Preparation and characterization of quantum-size titanium-dioxide*, J. Chem. Phys. **92**, 5196.
35. P. Pechukas (1969), *Time-dependent semiclassical scattering theory. I. Potential Scattering*, Phys. Rev. **181**, 166.
36. S.A. Haque et al. (1998), *Charge recombination kinetics in dye-sensitized nanocrystalline titanium dioxide films under externally applied bias*, J. Phys. Chem. B **102**, 1745.
37. S. Flores and V.S. Batista (2004), *Model Study of Coherent-Control of the Femtosecond Primary Event of Vision*, J. Phys. Chem. B **108**, 6745.
38. V.S. Batista and P. Brumer (2002), *Coherent Control in the Presence of Intrinsic Decoherence: Proton Transfer in Large Molecular Systems*, Phys. Rev. Lett. **89**, 143201.
39. S. Habib, W.H. Zurek and J.P. Paz (1993), *Coherent States via Decoherence*, Phys. Rev. Lett. **70**, 1187.
40. K. Bergmann, H. Theuer, and B.W. Shore (1998), *Coherent population transfer among quantum states of atoms and molecules*, Rev. Mod. Phys. **70**, 1003.
41. U. Hohenester and F. Troiani and E. Molinari and G. Panzarini and C. Macchiavello (2000), *Coherent population transfer in coupled semiconductor quantum dots*, App. Phys. Lett., **77**, 1864.
42. L.P. Yatsenko, V.I. Romanenko, B.W. Shore and K. Bergmann (2002), Stimulated Raman adiabatic passage with partially coherent laser fields, Phys. Rev. A, **65**, 043409.
43. M. Demirplak and S.A. Rice (2002), *Optical control of molecular dynamics in a liquid*, J. Chem. Phys., **116**, 8028.
44. Q. Shi and E. Geva (2003), *Stimulated Raman adiabatic passage in the presence of dephasing*, J. Chem. Phys., **119**, 11773.
45. G.S. Agarwal, M.O. Scully and H. Walther (2001), *Inhbition of decoherence due to decay in a continuum*, Phys. Rev. Lett. **86**, 4271.
46. G.S. Agarwal, M.O. Scully and H. Walther (2001), *Accelerating decay by multiple 2π pulses*, Phys. Rev. A **63**, 044101.
47. L. Viola and S. Lloyd (1998), *Dynamical suppression of decoherence in two-state quantum systems*, Phys. Rev. A **58**, 2733.
48. L. Viola, E. Knill and S. Lloyd (1999), *Dynamical decoupling of open quantum systems*, Phys. Rev. Lett. **82**, 2417.
49. D. Vitali and P. Tombesi (1999), *Using parity kicks for decoherence control*, Phys. Rev. A **59**, 4178.
50. W.M. Itano, D.J. Heinzen, J.J. Bollinger and D.J. Wineland (1990), *Quantum Zeno effect*, Phys. Rev. A **41**, 2295.
51. A.G. Kofman and G Kurizki (2000), *Accelaration of quantum decay processes by frequent observations*, Nature **405**, 546.
52. V.M. Axt and T. Kuhn (2004), *Femtosecond spectroscopy in semiconductors: a key to coherences, correlations and quantum kinetics*, Rep. Prog. Phys. **67**, 433.
53. H. Htoon, C.K Shih, T. Takagahara (2003), *Quantum coherence phenomena in semiconductor quantum dots: quantum interference, decoherence and Rabi oscillation*, Chaos, Solitons and Frac-

tals **16**, 439.
54. P. Zanardi and M. Rasetti (1997), *Error avoiding quantum codes*, Mod. Phys. Lett. B, **79**, 3306.